Optically Transparent Patch Antennas at 77 GHz Using Meshed Aluminum

Philipp Hügler[#1], Mohamad Zaky[#], Michael Roos[*2], Steffen Strehle[*2], and Christian Waldschmidt[#2]
[#]Institute of Microwave Engineering, Ulm University, 89081 Ulm, Germany
[*]Institute of Electron Devices and Circuits, Ulm University, 89081 Ulm, Germany
{[1]paul.huegler, [2]Forename.Familyname}@uni-ulm.de

***Abstract* — A process to realize optically transparent patch antennas with double-sided aluminum metalization of meshed structures on fused silica is presented in this paper. For cost-saving manufacturing, aluminum is used as metalization and wire-bonding is chosen as an industry standard RF interconnection technique. Despite the fact that aluminum has a lower conductivity compared to silver or gold, 64 % and 81 % transparent antennas at 77 GHz with 4.4 dBi and 3.7 dBi gain respectively were realized.**

***Keywords* — patch antennas, transparent antenna, millimeter wave technology, fused silica**

I. Introduction

The need for optically transparent antennas in the field of radar applications in various areas is constantly growing. Hand gesture control based on radar sensors is becoming increasingly popular and ranges from in car driver's hand recognition [1] to interaction with smartphones or wearables [2]. For all those applications, it is not desirable to hide the antenna behind a screen or within the frame, degrading the radiation performance significantly, but to embed it in the glass of the screen.

Various forms of optically transparent conductors are available such as Indium-tin-oxide (ITO) in mono- and multilayer arrangements or silver-coated polyester (AgHT) films. For these materials, the transparency is limited by the sheet resistance, rendering them as inadequate for antennas at RF frequencies [3]. To overcome this issue, a square-shaped metal mesh consisting of silver (Ag) and titanium (Ti) on glass substrates is introduced in [3] to realize transparent conductors with reasonable sheet resistance. To improve efficiency at millimeter-frequencies, [4] proposes to replace silver by gold (Au) on fused silica. The process is validated with a four-element transparent patch array with an overall transparency of 68 % at 77 GHz. For better support of the natural characteristic current modes, [5] introduces a honeycomb shaped grid structure on polyethylene terephthalate (PET) substrate featuring two-sided metalization and a VIA process.

In this paper the process parameters for a double-sided meshed metalization using aluminum (Al) and fused silica (JGS2) is presented. Regarding the required metalization thickness, which is here approx. 1 µm, aluminum is much cheaper compared to gold. Instead of probing, wire-bonding is tested as the interconnection between PCB and the glass samples. At first the effective dielectric constant of the substrate is measured using a ring resonator. After that, three different patch antennas, one opaque/fully metalized, 64 % transparent, and 81 % transparent are characterized in terms of input reflection coefficient and gain.

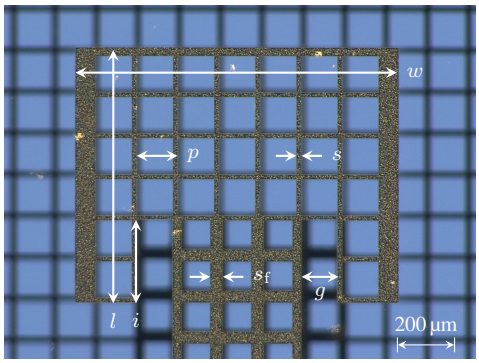

Fig. 1. Optical microscopy image of a fabricated patch antenna with 81 % transparency with a dense feeding line with 51 % transparency, including the design parameters (see Tab. 1).

II. Design and Fabrication

To realize optically transparent antennas, a quadratic meshed structure as proposed in [3] is used. The antennas examined in this paper are inset fed patch antennas. Fig. 1 illustrates a fabricated sample, with the design parameters patch length l, patch width w, clearance of the inset feed g, length of the inset feed i, pitch of the mesh p, strip width of the mesh s, and strip with of the feeding line s_f. The theoretical transparency is given by

$$T_\mathrm{grid} = \left(\frac{p-s}{p}\right)^2, \tag{1}$$

and the difference between the theoretical and measured value is less then 2 % according to [3]. As a second important design criterion, the theoretical sheet resistance $R_\square$ is calculated as in [3].

A 50 Ω line has a width of 435 µm on the used substrate material. All metal structures (patch, feeding line, and ground plane) are meshed with the same pitch and strip width, unless otherwise noted. Based on the dimensions of the solid patch, the pitch and strip width are chosen in order to build the structure with as many whole unit cells as

ISBN 978-3-9812668-9-4

Table 1. Physical dimensions of the fabricated solid antenna, 64 % transparent antenna, and 81 % transparent antenna with 51 % transparent feeding line.

Antenna	l in µm	w in µm	g in µm	i in µm	p in µm	s/s_f in µm	$R_\square$ in Ω/□
Solid	975	1190	150	310	-	-	0.026
64 % tr.	885	1130	125	290	140	28/28	0.132
81 % tr.	868	1100	125	284	140	14/40	0.263/0.092

possible and to realize the desired transparency. Tab. 1 summarizes the parameters for the investigated solid, 64 % transparent, and 81 % transparent patch antennas resulting from 3D electromagnetic field simulations. The antennas are simulated centered on the final structure size of 6 mm × 6 mm but without the PCB and the interconnection using wire bonds.

A. *Fabrication Process*

Before the fabrication process is introduced, the requirements are specified. Fused silica (JGS2) with a permittivity of ϵ_r=3.81 and a dielectric loss tangent $\tan(\delta)$=0.001 at 120 GHz [6] is used as the transparent substrate. The thickness of 200 µm is selected as a trade-off between surface wave excitation [7], mechanical stability, and cost. As metal for thermal evaporation aluminum is chosen due to its excellent adhesive properties, low cost, reasonable conductivity ($3.8 \cdot 10^7$ S/m), and lower evaporation temperature than gold (Au). Al is also preferred over copper (Cu) because of its better wire-bonding characteristics and bond reliability. For low losses, the deposited metal must be thicker than three times the skin depth, resulting in a film thickness of approx. 1 µm. To realize the transparency with a mesh structure, the minimum realizable structure size should be less 10 µm and the accuracy better than ±1 µm. In addition, a double-sided metalization is needed.

The single steps of coating, exposure, and metalization are described next. For all fabricated samples, 2 inch wavers are used and all steps are carried out in a class ISO-3 cleanroom. Top and bottom metalization are done sequentially. In case of a structured bottom layer (meshed ground plane), the bottom layer is metalized first, and the top layer containing the antenna design second.

Bilayer coating is used to achieve a 2 µm thick photoresist and to improve the lift-off. LOR 7b (lift-off resist) serves as an underlayer and AZ 5214E as the reactive photoresist. Both layers are spin-coated and the process parameters are listed in Tab. 2.

Exposure is done with a maskless direct-writing laser photolitography (Heidelberg µPG 101) working with a laser exposure wavelength of 375 nm. It can achieve a minimal feature size of 1 µm, offers automated alignment methods, which are required for double-sided metalization, and is ideal for rapid prototyping. Because reflections and scattering at

Table 2. Photolithography recipe for top and bottom layer.

	Speed	Time	Baking
LOR 7b	2000 rpm	60 s	180 °C for 320 s
AZ 5214E	4000 rpm	60 s	110 °C for 120 s

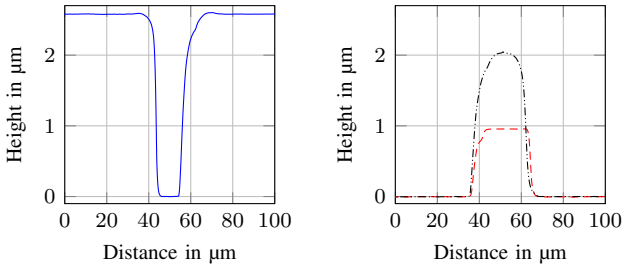

Fig. 2. Height profile measured with a stylus profilometer for (a) the developed (——) photoresist, (b) metalization of 1 µm (- - - -) evaporated Al, and 2 µm (-·-·-) sputtered Al.

the metallic structure lead to a photoresist overexposure, the exposed energy of the laser (power and pulse duration) has to be adjusted depending whether one side is already metalized (10 mW, 25 %) or not (40 mW, 25 %). The resist is developed in AZ 726 MIF developer for 42 s. Oxygen plasma etching is used to remove any residues of photoresist prior metalization. The measured thickness of a developed and plasma etched photoresist is shown in Fig. 2 (a). It is approx. 2.6 µm high and is therefore sufficient to realize the desired metalization thickness.

Metalization is done with two different methods, evaporation deposition and sputtering. For either method, a 10 nm titanium layer, acting as an adhesive layer between the glass and the Al, is deposited. The process is completed with the lift-off using N-Ethylpyrrolidone (NEP) and a ultrasonic bath. Both methods were successful, however sputtering showed better lift-off and adhesion to the substrate, which is why it was the method of choice for all presented designs.

The achieved metalization thickness is depicted in Fig. 2 (b). The intended film thickness of 1 µm for evaporation and 2 µm with sputtering result in 0.97 µm and 2.04 µm, respectively. Evaluating the accuracy of the process shows errors of less than 0.2 µm and a displacement between the top and bottom layer in the range of 5 µm to 10 µm as can be seen in Fig. 3. The offset is due to focusing difficulties of the alignment structures through the glass substrate. A rotational offset is not observed. The process requirements are therefore fulfilled.

III. Characterization

For characterization, a multilayer printed circuit board (PCB) build up of a FR4 carrier and RO3003 RF-substrate

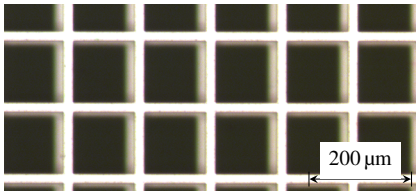

Fig. 3. Visible offset between top and bottom metalization of fabricated patch antenna with theoretical pitch p of 140 µm and strip width s of 20 µm.

ISBN 978-3-9812668-9-4

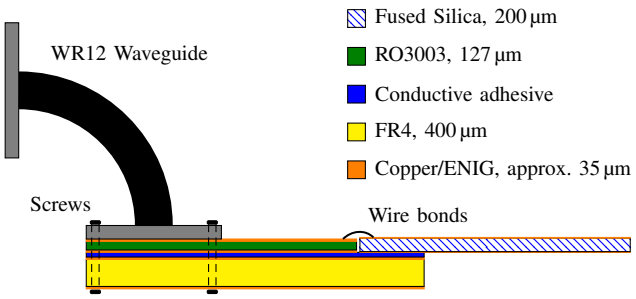

Fig. 4. Material stack-up of the used measurement set-up.

is used. A cavity is formed by cutting out the RO3003 layer, in which the glass samples are glued in with a silver filled electric conductive adhesive. The microstrip line traces are interconnected using triple wire bonds. The connection to the measurement equipment is achieved using a WR12 waveguide-to-microstrip line (WG-to-MSL) transition covering the complete frequency range from 60 GHz to 90 GHz. In case of transparent structures, only a small part (1 mm) between the glass and the FR4 carrier are overlapping, as can be seen in Fig. 4.

The reference plane for scattering parameter measurements is set on the glass substrate by applying a TRL (through, reflect, line) calibration on glass to calibrate out the influence of the WG-to-MSL transition and wire bonds. The gain is measured in an anechoic chamber with a 25 dBi standard gain horn as the reference antenna. For all measurements, the measurement bandwidth is set to 100 Hz.

A. Material Characterization

In order to characterize the effective permittivity $\epsilon_{r,\mathrm{eff}}$ of the used glass material, a microstrip line ring resonator is used. Based on the designed length l_m of the resonator, the effective permittivity $\epsilon_{r,\mathrm{eff}}\left(f_{\mathrm{R},n}\right)$ can be determined at the discrete resonance frequencies $f_{\mathrm{R},n}$ [8]. This is based on the relation of the middle diameter of the ring D_m and the multiples n of the guided wavelength $\lambda_{\mathrm{R},n}$

$$l_m = \pi D_m = n\lambda_{\mathrm{R},n}. \tag{2}$$

By rearranging, $\epsilon_{r,\mathrm{eff}}\left(f_{\mathrm{R},n}\right)$ can be extracted:

$$\epsilon_{r,\mathrm{eff}}\left(f_{\mathrm{R},n}\right) = \left(\frac{c_0 n}{\pi f_{\mathrm{R},n} D_m}\right)^2. \tag{3}$$

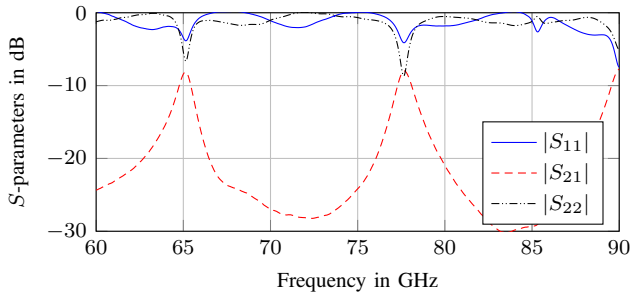

Fig. 5. S-parameters of characterized ring resonator.

For higher accuracy it must be taken into account, that equations (2) and (3) are valid for a lossless resonator. Because of that, the quality factor Q must be considered

$$f_{\mathrm{R},n} = f_{\mathrm{R},n}^{(m)}\left(1 - \frac{1}{2Q}\right)^{-1} \tag{4}$$

with $f_{\mathrm{R},n}^{(m)}$ representing the measured resonant frequency. Q can be determined with the loaded quality factor Q_L — which depends on the relation between the resonance frequency and the 3 dB bandwidth of the resonance Δf_n — and the insertion loss $|S_{21}\left(f_{\mathrm{R},n}\right)|$ as described in [8].

The ring resonator is designed for 77 GHz and D_m is chosen as 4.2 mm, resulting in n=6. Measurement results are depicted in Fig. 5 and $f_{\mathrm{R},6}^{(m)}$=77.64 GHz, Δf_6=1.03 GHz, and $|S_{21}\left(f_{\mathrm{R},n}\right)|$=−8.0 dB can be extracted. Using the above equations $\epsilon_{r,\mathrm{eff}}$ at 77.64 GHz results in 3.14. This is in good accordance with the $\epsilon_{r,\mathrm{eff}}$=3.2 calculated in the used 3D electromagnetic simulation software.

B. Antenna Characterization

Starting with the fully metalized patch antenna, the measured and simulated input reflection coefficients $|S_{11}|$ are compared in Fig. 6 (a). The resonance frequency measures approx. 75 GHz and a −10 dB bandwidth of 2.5 GHz is achieved. The shift of 2 GHz in the resonance frequency can directly be explained with the difference between the assumed and measured effective permittivity described previously. The results for the gain measurements are compared at the antennas corresponding resonance frequency. The losses of the WG-to-MSL transition as well as the losses of the wire bonds are de-embedded. The H-plane results are depicted in Fig. 6 (b) and are in good accordance to the simulation results. The maximum gain is 5 dBi and the half-power beamwidth (HPBW) results in 70°.

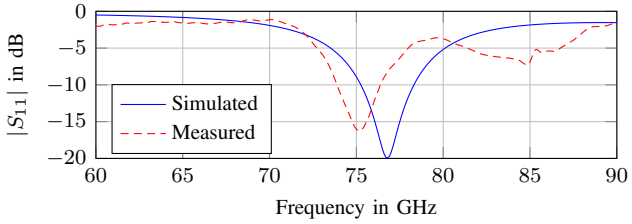

(a)

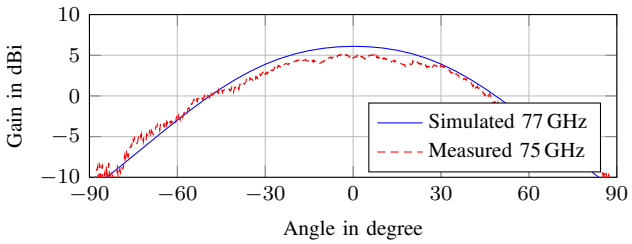

(b)

Fig. 6. Fully metalized patch antenna, (a) input reflection coefficient, and (b) gain in the H-plane.

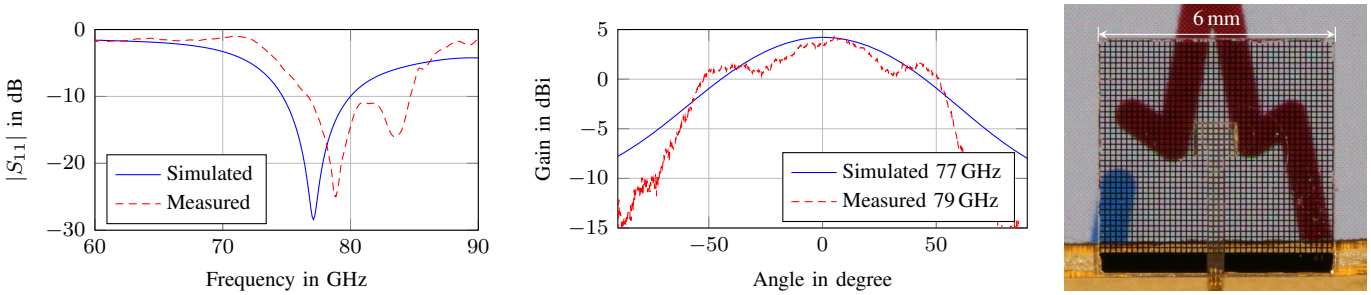

(a) (b) (c)

Fig. 7. Patch antenna with 64 % transparency, (a) input reflection coefficient, (b) gain in the H-plane, and (c) a photograph of the antenna located on a display.

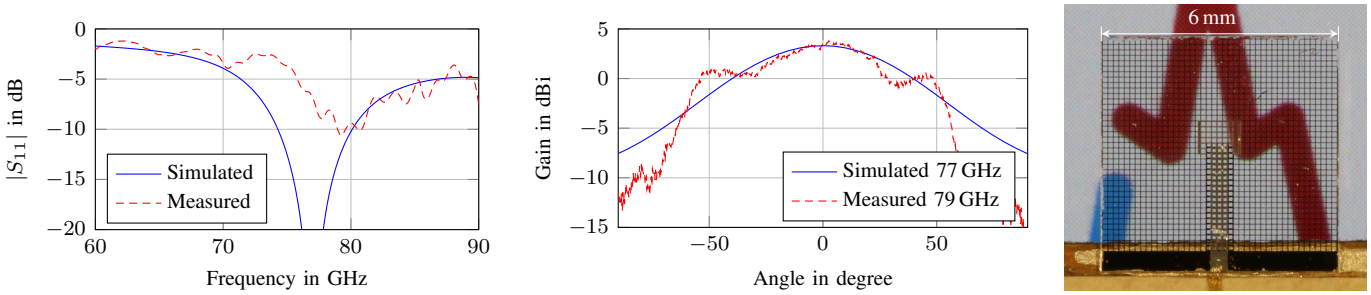

(a) (b) (c)

Fig. 8. Patch antenna with 81 % transparency and dense feeding network with 51 % transparency, (a) input reflection coefficient, (b) gain in the H-plane, and (c) a photograph of the antenna located on a display.

The results of the 64 % transparent antenna are depicted in Fig. 7. Again, a frequency shift of approx. 2 GHz of the resonance frequency (79 GHz) can be observed, but in this case in the opposite direction. This behavior can be reproduced for antennas with 81 % transparency (see Fig. 8) and in simulations by adjusting the permittivity. Comparing the simulated and measured gain, the H-plane cut shows a measured gain of 4.4 dBi and a HPBW of approx. 50°. This implies, that a transparent design can achieve comparable performance to a fully metalized patch.

For further increasing the transparency, a mesh with 81 % transparency is used. To reduce losses of the feeding line, the mesh of the feeding line itself and of the ground plane directly below the feeding line is made more opaque (51 % transparent) as depicted in Fig. 1. The difference between the assumed permittivity and measured permittivity influences this design more drastically and the input reflection coefficient depicted in Fig. 8 (a) is distorted a lot. The measured gain is shown in Fig. 8 (b) and results in 3.7 dB at 79 GHz and the HPBW is approx. 50°. The increased transperancy is clearly visible when both antennas are located on a display, cf. Fig. 7 (c) and Fig. 8 (c).

IV. Conclusion

The realization of transparent antennas using low-cost Al on fused silica has been shown. Interconnections between a PCB and the antennas on glass substrate using standard wire bonding technique has proven to be reliable. Despite Al has lower conductivity compared to Au and Ag, inset fed solid, 64 %, and 81 % transparent patch antennas with gains of 5.0 dBi, 4.4 dBi, and 3.7 dBi have been achieved. For the solid and 64 % transparent antennas, a −10 dB bandwidth of more than 2.5 GHz could be achieved.

Acknowledgment

This work was partly supported by the Ministry for Science, Research, and Arts Baden-Württemberg within the project ZAFH MikroSens. The support with the fabrication process by Stefan Jenisch is also gratefully acknowledged.

References

[1] P. Molchanov *et al.*, "Multi-sensor System for Driver's Hand-Gesture Recognition," in *11th IEEE International Conference and Workshops on Automatic Face and Gesture Recognition*, vol. 1, May 2015, pp. 1–8.

[2] J. Lien *et al.*, "Soli: Ubiquitous Gesture Sensing with Millimeter Wave Radar," *ACM Trans. Graph.*, vol. 35, no. 4, pp. 142:1–142:19, Jul. 2016.

[3] J. Hautcoeur *et al.*, "Transparency and electrical properties of meshed metal films," *Thin Solid Films*, vol. 519, no. 11, pp. 3851 – 3858, 2011.

[4] J. Hautcoeur *et al.*, "60 GHz optically transparent microstrip antenna made of meshed AuGL material," *Microwaves, Antennas Propagation, IET*, vol. 8, no. 13, pp. 1091–1096, Oct. 2014.

[5] H. Sharifi *et al.*, "Semi-Transparent and Conformal Antenna Technology for Millimeter-wave Intelligent Sensing," in *IEEE MTT-S International Conference on Microwaves for Intelligent Mobility*, Apr. 2018, pp. 1–4.

[6] M. N. Afsar and K. J. Button, "Millimeter-Wave Dielectric Measurement of Materials," *Proc. of the IEEE*, vol. 73, no. 1, pp. 131–153, Jan. 1985.

[7] D. M. Pozar, "Microstrip Antennas," *Proceedings of the IEEE*, vol. 80, no. 1, pp. 79–91, Jan. 1992.

[8] R. Hoffmann and H. Howe, *Handbook of Microwave Integrated Circuits*. Artech House, 1987.